Journal of Water Process Engineering 50 (2022) 103312

Contents lists available at ScienceDirect

Journal of Water Process Engineering

journal homepage: www.elsevier.com/locate/jwpe

Development of novel nano-γ-Al_2O_3 adsorbent from waste aluminum foil for the removal of boron and bromide from aqueous solution

Mohammad A. Al-Ghouti [a,*], Mariam Khan [a], Aakasha Malik [b], Majeda Khraisheh [b], Dima Hijazi [a], Sana Mohamed [a], Shaikha Alsorour [a], Razan Eltayeb [a], Fay Al Mahmoud [a], Johaina Alahmad [a]

[a] Environmental Science Program, Department of Biological and Environmental Sciences, College of Arts and Sciences, Qatar University, Doha, Qatar
[b] Department of Chemical Engineering, College of Engineering, Qatar University, P.O. Box 2713, Doha, Qatar

ARTICLE INFO

Keywords:
Remediation
Alumina
Waste management
Water treatment
Water reuse
Spent adsorbent

ABSTRACT

The current study deals with the synthesis of nano-gamma-alumina (nano-γ-Al_2O_3) from waste aluminum foil and its application for the removal of boron and bromide from an aqueous solution. The physical characteristic of nano-γ-Al_2O_3 was analyzed using various analytical techniques, namely thermogravimetric analyzer (TGA), scanning electron microscope (SEM), energy dispersive X-ray (EDX), and Fourier-transform infrared spectroscopy (FTIR). Additionally, various important parameters that govern the adsorption process were examined, such as pH, solution temperature, and initial ions concentration. It was found that boron preferred a basic environment while bromide prefers a less acidic environment. The prepared adsorbent also demonstrated a very high removal efficiency; 88.35 % of boron and 87.65 % of bromide were achieved. Isotherm studies showed that the Langmuir model best explained the adsorption processes for both boron and bromide at 25 °C. The maximum boron and bromide adsorption capacities (Langmuir adsorption capacity) were 25.86 mg/g (at 35 °C) and 90.72 mg/g (at 25 °C), respectively. Moreover, the evaluated thermodynamic parameters revealed that boron followed an endothermic reaction while bromide followed an exothermic reaction. The ΔG° value for both ions indicated that adsorption was favorable. While the kinetic studies revealed that both, boron and bromide adsorption onto nano-γ-Al_2O_3 obeyed pseudo-second-order; indicating that electrostatic forces and electron sharing would be amongst the major forces involved in the adsorption process. The desorption experiments confirmed that the spent adsorbents can be regenerated and effectively reused. The prepared nano-γ-Al_2O_3 was also tested with a real groundwater sample, and it was found that 96.25 % of boron and 100 % of bromide were successfully adsorbed using nano-γ-Al_2O_3. Additionally, it was also found that 99 % of sulfate ions were removed. This showed that the prepared adsorbent has the tendency to adsorb multiple ions from the real groundwater sample.

1. Introduction

Due to limited water resources, several countries have relied on seawater desalination technology to meet their water needs. Desalination of seawater has become an unavoidable trend in a variety of industries, including agricultural and industrial production, as well as the daily existence of living organisms and plants [1]. In seawater, boron concentration usually varies between 5 mg/L and 6 mg/L [2]. Though boron is considered an essential micronutrient for humans, plants, and animals, a however excessive amount of boron has been reported to cause an adverse effect on both plants and animals [3]. According to World Health Organization (WHO), 1 mg/day to 20 mg/day is the maximum acceptable amount of boron uptake [4]. Pharmaceuticals, condensers, detergents, preservatives, enamel, leathers, carpets, fertilizers, artificial gemstones, and high-contrast photogenic materials are just a few of the products that expose their customers to roughly 0.1 mg of boron each day [5]. Many countries have specified a limit to boron level in irrigation water that must be maintained (<1 mg/L) to reduce boron poisoning in plants as they may lose their photosynthetic potential and productivity if the amount is too high [5]. However, some plants can sustain high boron concentrations (2 mg/L to 4 mg/L) in irrigation water, while other very sensitive or semi-sensitive plants, can tolerate up to 0.3 mg/L, and 1 mg/L to 2 mg/L, respectively. It has also been reported to affect the blood and endocrine system in adults, there has been

* Corresponding author.
E-mail address: mohammad.alghouti@qu.edu.qa (M.A. Al-Ghouti).

https://doi.org/10.1016/j.jwpe.2022.103312
Received 15 April 2022; Received in revised form 30 October 2022; Accepted 2 November 2022
Available online 11 November 2022

an increase in incidents of pregnancy complications, and congenital malformation, which has been linked to boron toxicity [6–10]. Due to its severity, WHO has set a maximum for boron concentration in drinkable water, which must be <2.4 mg/L [11]. The non-ionic form of boron in seawater production cannot be treated by a simple desalination plant procedure and demands a more complex method [8]. On the other hand, bromide is also abundant in natural water, particularly in water bodies due to anthropogenic activities such as the discharge of treated or untreated wastewater and power plant discharges [9]. Bromide ion is also another element that is known to be toxic to mammals, aquatic organisms, and plants. It is considered to cause carcinogenicity, as well form trihalomethanes, cause toxicity to the reproductive system and affects the development of bodies. Additionally, neurotoxicity and other acute organ toxicity are some of the other common side effects of excessive bromide consumption [10]. In seawater, bromide concentration can range between 65 mg/L and 80 mg/L [11]. Due to ozonation and chlorination, when bromide ion dissolves in water, it forms a toxic chemical that can harm the ecosystem and cause cancer and other chronic diseases in humans [12]. Additionally, bromide ions existing in water can respond differently to different disinfectants [13]. During the pre-chlorination process, a high amount of chlorinated disinfection by-products (DBPs), particularly (Cl-DBPs) and (Br-DBPs) can be produced from seawater containing a high amount of bromide ions (50 mg/L–80 mg/L), which are extremely harmful [14]. Furthermore, natural processes such as the movement of saline water into freshwater aquifers, erosion of rocks, as well as anthropogenic activities including seawater desalination, mining tailings, chemical reactions, sewage, and industrial discharge, are some of the sources of bromide in drinking water [15].

The need to regulate the presence of boron and bromide in water has been recognized by several studies, which have presented several efficient ways for removing these ions from aqueous solutions. Some of the technologies that have been presented as possible technologies to treat boron and bromide ions include electrocoagulation [16], ion exchange [17], reverse osmosis [18], and adsorption [19]. However, there are various limitations associated with the high percentage removal of boron and bromide when using electrocoagulation, ion exchange, and reverse osmosis. Such as the generation of toxic by-products, and volatilization, the construction of the plant, requires a large area, can cause fouling and scaling, and can deteriorate water quality. Over the years, adsorption has emerged as a superior technique owing to its cost-effectiveness, selectivity, and comparatively environmentally friendly alternative. Accordingly, the exploitation of various dross that is produced by industries has also emerged as the greatest challenge for the industries [20]. Usually, the waste is disposed of in designated landfills, which is likely to cause the leaching of toxic metal ions into the groundwater causing serious pollution problems, additionally; landfills require large land, which is also one of the main concerns due to increasing production [21]. Utilizing such waste from another industry could be one of the possible ways to save operational costs. Owing to its environmental friendliness and strong adsorption capacities, the use of recycling waste material for boron and bromide removal from an aqueous solution has gotten a lot of attention [19]. Aluminum has gained great attention since it is dumped as a waste by-product from various industries on daily basis. Additionally, nanomaterials of aluminum oxide and aluminum hydroxide are extensively studied due to their hierarchal nanostructure and unique properties. Currently, several methods have been proposed to successfully prepare alumina [22–23].

The current study aimed to prepare nano-γ-Al_2O_3 using waste aluminum foil through a hydrothermal process. The synthesis of alumina was carried out in an acidic preparation using hydrochloric acid (HCl) and drops of ammonia. HCl is an inexpensive raw material and ammonia was only required in a few drops. The physical and chemical properties of the prepared nano-γ-Al_2O_3 were analyzed using various analytical techniques. The effect of various essential parameters on boron and bromide adsorption was also evaluated. Four isotherm models namely, Langmuir, Freundlich, Dubinin–Radushkevich, and Temkin were used to evaluate the boron and bromide adsorption processes, and thermodynamics studies were performed to understand the adsorption process pathway.

2. Methodology

2.1. Synthesis of nano-aluminum oxide, nano-γ-Al_2O_3

The preparation procedure of nano-γ-Al_2O_3 was modified by Osman et al. [22]. The aluminum foil wastes were collected, washed, and stored in airtight containers. 6 M of HCl solution was added to 20 g of aluminum foil and stirred to form an $AlCl_3$ solution. The mixture was maintained in a desiccator for 24 h to form crystalline $AlCl_3.6H_2O$, then deionized water was used to purify the $AlCl_3.6H_2O$, to assure the purity of the $AlCl_3.6H_2O$ crystals, washing was carried out three times [22,23]. The prepared $AlCl_3.6H_2O$ were dissolved in deionized water and heated up to 100 °C and ammonia solution (35 %) was added gradually to form a pale off-white precipitate, which was kept at room temperature for 12 h. The precipitate was filtered (centrifuged), washed, dried, and calcined at 550 °C for 4 h. The final product (nano-γ-Al_2O_3) was crushed and kept in a sealed container. Fig. 1 displays a schematic illustration of the procedure carried out to achieve nano-γ-Al_2O_3.

2.2. Materials characterization

All chemicals used in this study were analytical grade. The prepared nano-γ-Al_2O_3 were characterized using various instruments. Thermogravimetric Analyzer (TGA) (Perkin Elmer TGA-4000, USA) was used to measure the thermal characteristics of nano-γ-Al_2O_3 at a heating rate of 15 °C/min in the presence of a 20 mL/min N_2 flow as an inert gas. Functional groups were determined by using Fourier-transform infrared spectroscopy (FTIR) PerkinElmer 400 Spectrum instrument using UATR (Universal Attenuated Total Reflectance). X-ray photoelectron spectroscopy (XPS) analysis was performed using Axis (Ulta DLD XPX Kratos, Manchester, UK) with Al Ka radiation source (1486.6 eV) X-ray Powder, 15 kV, 20 mA under a UHV environment. The physical morphology of the prepared nano-γ-Al_2O_3 was determined by scanning electron microscope (SEM) and energy dispersive X-ray (EDX); NovaTM Nano SEM 50 Series (FEI SEM, Quanta 200, USA) and transmission electron microscope (TEM) (Nanomeasurer 1.2, H-7650 Hitachi, Japan TEM). While the surface area and pore size distribution were determined by Brunauer-Emmett-Teller (BET) (Quantachrome Corporation, Nova 3000). To determine boron and bromide concentrations in an aqueous solution, inductively coupled plasma optical emission spectrometer (ICP-OES) Perkin-Elmer Optima 3000 V and ion chromatography (IC); Shimadzu ICPS-7510 Sequential Plasma Spectrometer (Japan) were used.

2.3. Stock solution preparation

100 mg/L of boron and bromide stock solution was prepared. Then the stock solution was diluted to the desired concentrations (10, 20, 30, 40, 50, 60, 80, 90, and 100 mg/L). IC and ICP-OES were used to determine the concentrations of bromide and boron in each solution respectively.

2.4. Adsorption studies

The experiments were performed in batches to determine the adsorption capacities of the prepared nano-γ-Al_2O_3 for boron and bromide ions. In this study, various parameters were investigated such as the influence of pH, initial ions concentration, and solution temperature. The batch experiment was carried out by adding 0.05 g of the prepared adsorbent to 50 mL of the stock solution, which was placed in a 100 mL glass bottle (previously soaked in acid). The bottles were placed in a shaker at room temperature, for 24 h at 165 rpm. To determine the effect

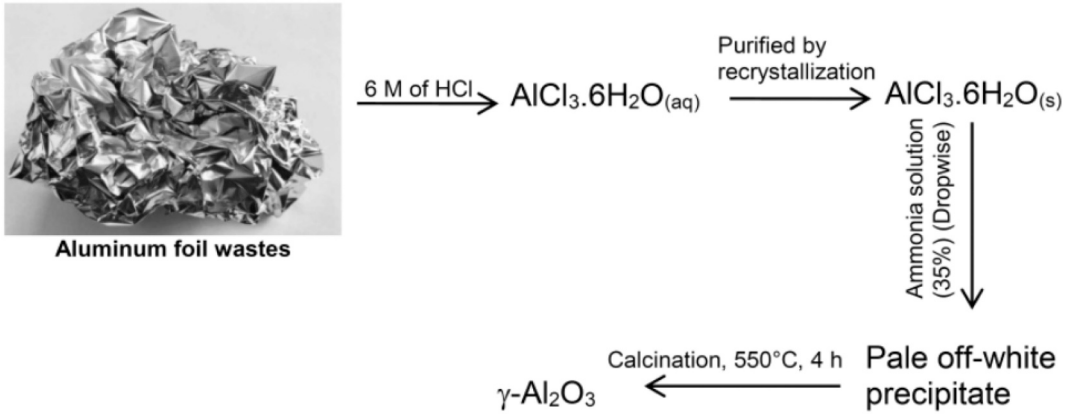

Fig. 1. Proposed schematic illustration of nano-γ-Al_2O_3 preparation from aluminum foil waste.

of pH, samples of boron and bromide solution were adjusted to different pH values (2, 4, 6, 8, and 10). The pH was adjusted by adding 0.05 M NaOH and 0.05 M HCl as needed. Moreover, the effect of temperature was also tested at various temperatures (25 °C, 35 °C, and 45 °C). Lastly, the effect of concentration was tested at 10 different concentrations (10 mg/L–100 mg/L). After each experiment, the samples were centrifuged (7000 rpm), and the solution was analyzed using ICP-OES for boron and IC for bromide. The percentage removal was calculated using the following equation. Duplicates and blanks were prepared in each experimental set to validate the data.

$$\%\text{Removal}\ (\%) = \frac{C_0 - C_e}{C_0} \times 100 \tag{1}$$

The initial concentration (mg/L) and the final concentration (mg/L) were denoted by C_0 and C_e, respectively.

2.5. Adsorption isotherm

Four isotherm models were used to evaluate the adsorption capacity, namely Langmuir, Freundlich, Temkin, and Dubinin-Radushkevish. The equation and parameter of each isotherm model can be found in the supplemental file (Fig. S1). In addition, the maximum adsorption capacity was calculated using Langmuir constant Q°_{max}.

2.6. Thermodynamics study

Thermodynamic analysis was also performed to understand the nature of the adsorption reaction by determining the changes in the parameters including Gibbs free energy (ΔG^o), entropy (ΔS^o), and enthalpy (ΔH^o) using the following equation:

$$\Delta G^o = -RT\ ln\ K_d \tag{2}$$

$$K_d = \frac{q_e}{C_e} \tag{3}$$

where R is the gas constant 8.314 J/mol. K, T is the temperature in Kelvin, and K_d is the distribution coefficient. Where C_e is the equilibrium concentration of the adsorbent in mg/L and q_e is the amount of boron or bromide adsorbed per gram during adsorption in mg/g.

$$\Delta G^o = \Delta H^o - T\Delta S^o \tag{4}$$

where ΔG^o is Gibbs free energy (kJ/mol), T is the temperature in Kelvin (K), ΔS^o is the entropy change (J/mol.K) and ΔH^o is the enthalpy (kJ/mol).

Additionally, adsorption affinity (R_L) was also calculated using Eq. (5). R_L indicates whether a reaction was favorable or not. Values above 1 indicate the reaction was linear while the R_L value denoted by zero indicates the reaction was irreversible.

$$RL = \frac{1}{1 + K_d C_0} \tag{5}$$

where C_0 is the initial concentration of the ions (mg/L).

2.7. Kinetic studies

The kinetic and thermodynamic equilibrium investigations were developed based on the conditions established in earlier experiments. To conduct the kinetic investigation, 0.5 (*w/v*) dried adsorbent was added to a 1.5 L boron or bromide solution with a known concentration. There were fifteen different contact times: 0, 1, 3, 5, 10, 15, 20, 30, 40, 50, 60, 90, 120, 240 and 300 min. Some of the most common kinetic models, namely pseudo-first-order, pseudo-second-order, and intra-particle diffusion models were used for the kinetic study. The mathematical formulas in Eqs. (6), (7), and (8), respectively provide the relationships between the solid and liquid phase concentrations (Ho and McKay, 1998; Ho and McKay, 2000).

$$q_t = q_e\left(1 - e^{-k_1 t}\right) \tag{6}$$

Pseudo-second-order kinetic equation

$$q_t = \frac{k_2 {q_e}^2 t}{1 + k_2 {q_e}^2 t} \tag{7}$$

where q_t is the adsorption quantity (mg/g), qe is the adsorption quantity of different samples at equilibrium (mg/g) refers to; t is time (h); k_1 (1/min) and k_2 (g/mg.min) stand for the adsorption rate constants of pseudo-first-order and pseudo-second-order, respectively.

Weber-Morris intra-particle diffusion

$$q_t = k_{id} t^{0.5} + B \tag{8}$$

The slope and intercept of the linear plots are used to derive the intra-particle diffusion parameters (rate constants and equilibrium concentrations). B is the intercept associated with the boundary layer which is obtained from the intercept while k_{id} is the rate constant related to internal diffusion (mg/g.$min^{0.5}$) and which is determined from the slope of the graph when q_t is plotted against the $t^{0.5}$ plot.

2.8. Reusability of the adsorbent

The separation of the spent nano-γ-Al_2O_3 for the removal of 100 ppm boron and bromide solution was achieved by centrifuging each sample for 30 mins. Then, the spent material was washed carefully, to minimize any loss. It is essential to wash the spent adsorbent to ensure the removal of any boron and bromide ions that may not be adsorbed by nano-

γ-Al_2O_3. Various eluents including HCl were used for the desorption process, in which a set concentration of the acid was added to the glass bottle to which the spent nano-γ-Al_2O_3 was added. The bottles were kept in the incubator shaker at room temperature for 24 h, 165 rpm then centrifuged for 30 min.

2.9. Desorption study

To investigate the desorption capacity of spent adsorbent (nano-γ-Al_2O_3) that had already adsorbed boron and bromide, three initial concentrations of 40 mg/L, 70 mg/L, and 100 mg/L were used. Two separate solutions were used to evaluate the spent adsorbents: 0.5 M HCl and 1 M HCl in 100 mL glass bottles. 0.05 g of spent nano-γ-Al_2O_3 of boron was added to 50 mL of each solution. Replicate experiments were carried out. The mixture was then shaken at 165 rpm for 24 h at room temperature. After each experiment, the samples were centrifuged (7000 rpm), and the solution was analyzed using ICP-OES for boron and IC for bromide. The desorption percentage was calculated according to the following Eq. (9):

$$\text{Desorption}\ (\%) = \frac{C_0 - C_e}{C_0} \times 100 \tag{9}$$

where C_0 is the initial concentration based on the average adsorption (mg/L) and C_e is the equilibrium concentration (mg/L).

2.10. Cost analysis

The estimated cost of the prepared nano-γ-Al_2O_3 was determined from the cost of the individual steps occurring during the preparation process of 1 kg nano-γ-Al_2O_3. This includes the chemicals cost, electricity consumption, and other overhead costs. All calculations were based on the adsorption capacity of the prepared nano-γ-Al_2O_3 for boron and bromide removal.

2.11. Statistical analysis

Two-way ANOVA was used to help understand the interaction of the independent variables with the dependent variable. Statistical analysis of all data was carried out in Excel. To validate the data, duplicates of all experiments were performed. Additionally, Chi-square $(\chi)^2$ and coefficient correlation (R^2) were used to investigate the best-fit adsorption isotherm model.

The Chi-square $(\chi)^2$ was calculated as the following Eq. (10):

$$\chi 2 = \sum_{i=1}^{N} \frac{\left(q_{exp}^{i} - q_{pred}^{i}\right)^2}{q_{pred}^{i}} \tag{10}$$

where, q_{exp}^{i} is the equilibrium capacity (mg/g) from the experimental data while q_{pred}^{i} is the equilibrium capacity (mg/g) from the predicted (model) data. The data were used from the results obtained from the effect of initial concentration. N denotes the number of sizes, which is the number of match experimental runs conducted to find out the adsorption capacity.

Accordingly the Critical value (*p*-value) for 10 is 18.31 at $\alpha = 0.05$. Therefore if the $(\chi)^2$ is lower than the p-value the null hypothesis is not rejected and it will be concluded that there is no sufficient evidence that the experimental value is different from the predicted value.

2.12. Adsorption of boron and bromide ions from groundwater using nano-γ-Al_2O_3

A real groundwater sample was used as a real wastewater sample to determine the efficiency of prepared nano-γ-Al_2O_3. The groundwater was collected from a local area. The experiment was carried out by adding 50 mL of the collected groundwater and 0.05 g of nano-γ-Al_2O_3. The solutions were agitated at 165 rpm at ambient temperature for 24 h. The solution was then centrifuged, and the equilibrium concentrations of boron and bromide were measured using ICP-OES and IC, respectively. The removal percentage was calculated using Eq. (1).

3. Results and discussion

3.1. Characterization of the prepared nano-γ-Al_2O_3

3.1.1. Morphological characterization using SEM

The intended purpose of conducting an SEM analysis of a sample was to attain a topological image of the compound and its relative composition. Figs. 2A and (S2a-d) provide the SEM images of the prepared nano-γ-Al_2O_3. It can be observed from Fig. 2A and B, that the adsorbent had several cavities, thus ensuring high adsorption capacity. The close clustering of the cavities is due to the oxidation that occurred at high temperatures. The roughness of the surface indicates the presence of impurities due to other components that may have been present in the aluminum foil. Additionally, the morphology of the prepared adsorbent is also observed as porous and heterogeneous. Such characteristics will indeed facilitate the capturing of boron and bromide. Similar findings were also reported by Zhang et al. [19] and Murambasvina & Mahamadi [24]. The presence of active sites on nano-γ-Al_2O_3 will influence the physicochemical properties of the adsorbent. The formation of the defective structure during the transition from amorphous to crystalline in a thermal dehydration state resulted in increased chemical and active adsorption sites. During the preparation of nano-γ-Al_2O_3, the interaction of water vapor on the aluminum surface is one of the most complex processes under the influence of various types of forces. The sharp edges formation may be due to the increase of γ-alumina content. The results from the EDX spectral elemental analyses of the adsorbent surface of aluminum oxide are shown in Fig. 2C. The purity of aluminum oxide is shown in quantitative measuring findings obtained from the EDX analysis. The EDX measurements indicate the presence of Al along with O peaks. The results indicated 57.53 % of O and 42.47 % of Al. Additionally, the use of precursor salts for nanoparticle production was responsible for the weaker signal of K. Overall, the results indicated the high purity of the adsorbent. Similar results were observed in various studies, for instance, Zhu et al. [25] prepared aluminum oxide adsorbent and obtained similar results, aluminum comprised 35.4 % wt%. On the other hand, Zhang et al. [19] found the content of nano-γ-Al_2O_3 to be 40.55 % Al, and 59.45 % O.

The structure and shape of the synthesized nano-γ-Al_2O_3 were further analyzed by TEM, which is shown in Fig. 2D & E. The TEM images make it easier to comprehend the regular layer and interlayer region present in the adsorbent. Fig. S3 depicts a wormhole-like structure, which is a distinct and common characteristic of nano-γ-Al_2O_3 reported in various studies including Lee et al. [26] and Ekka et al. [27]. Additionally, narrow pore size with a particle size of 500 nm can be observed throughout the surface as evident in Figs. 2D and E, and S3. In general, Fig. 2D and E also show that nano-γ-Al_2O_3 can be thought of as a laminar structure. Lastly, overall, it can also be seen that the nano-γ-Al_2O_3 structure is more homogenous and consistent. Similar findings were also reported by Cardona et al. [20] and Gómez et al. [28]. At the same time, it can be observed that the particles are found to be irregular which indicates particle crystalline feature, which is another distinct property of nano-γ-Al_2O_3 [29].

3.1.2. Surface area analysis

Adsorption rate and adsorption capacity are influenced by the adsorbent's surface area. The BET analysis revealed that nano-γ-Al_2O_3 possessed a high surface area of 150.0 m^2/g compared to other studies. While the pore volume and pore sizes were 0.208 cm^3/g and 27.20 Å, respectively. The pore area distribution and nitrogen adsorption-desorption isotherms graphs are presented in Fig. S4, a supplementary document. For instance, Lee & Lee [30] reported the surface area of the

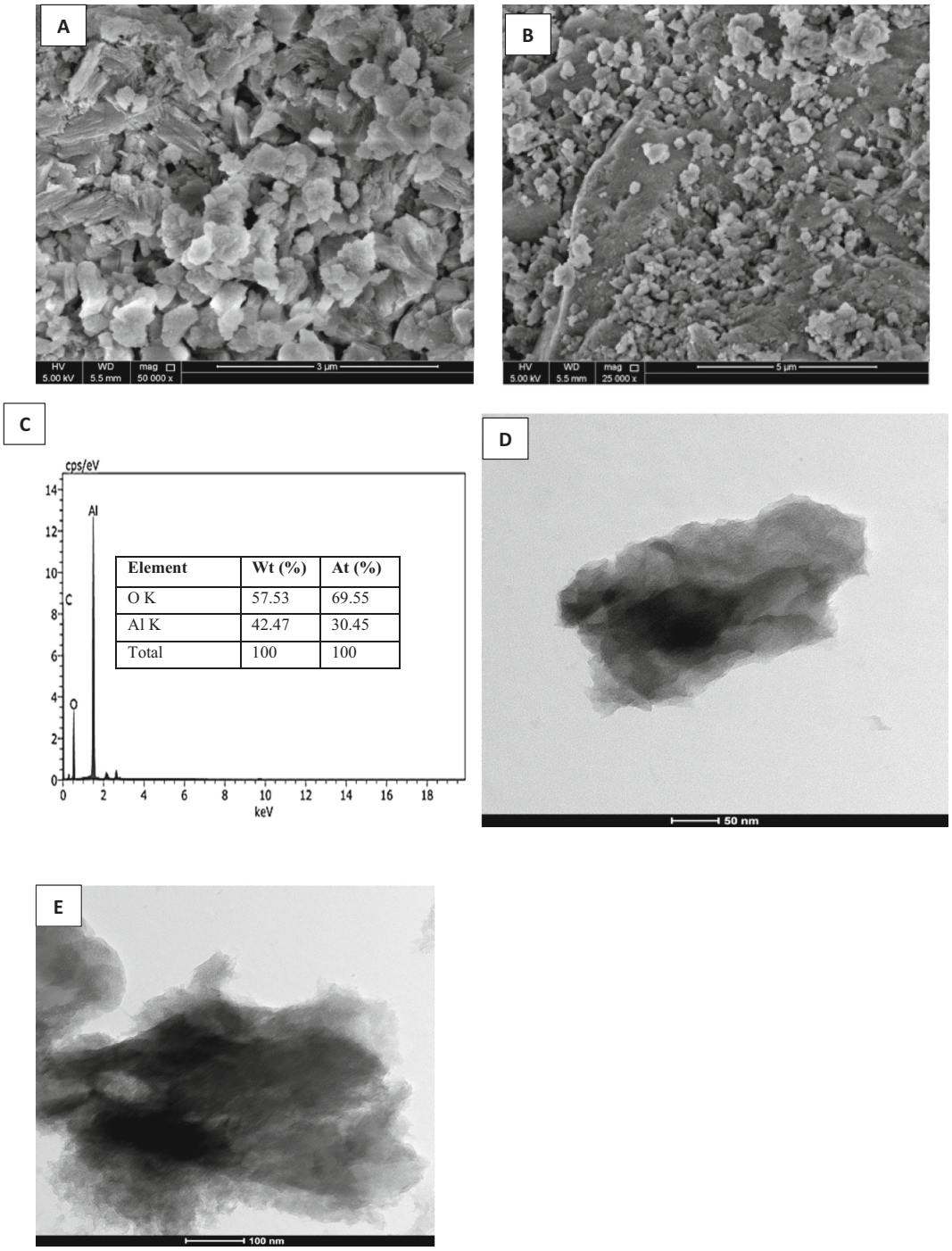

Fig. 2. A and B: The scanning electron microscope (SEM) image, of nano-γ-Al_2O_3 before adsorption at ×50,000 & 25,000. C. Corresponding energy, dispersive spectrum (EDX) pattern, and D and E: TEM images for the prepared nano-γ-Al_2O_3 before adsorption.

prepared aluminum oxide particles as 46.80 m^2/g. While Zhu et al. [25] reported the surface area of the prepared mesoporous bismuth-impregnated aluminum oxide between 107 m^2/g and 161.0 m^2/g and pore volume between 0.196 cm^3/g–0.301 cm^3/g. Zhang et al. [31] synthesized γ-aluminum oxide and recorded a surface area between 58.60 m^2/g–85.30 m^2/g.

3.1.3. *Fourier Transform Infrared Spectroscopy (FTIR)*

The results obtained through the FTIR analysis display peaks that correspond to the presence of aluminum oxide can be observed in Fig. 3. Several peaks between 400 cm^{-1}–1000 cm^{-1} determined the formation of γ-phase alumina. For instance, the peak at 880 cm^{-1} indicated asymmetric stretching, 795 cm^{-1} showed symmetric stretching, and 630 cm^{-1} showed the bending vibrations of the Al—O—Al bonds. Lastly, the presence of an octahedral arrangement of the Al^{3+} peak was determined by the peak present at 680 cm^{-1} [32]. The peak observed at 1101 cm^{-1} and 611 cm^{-1} is attributed to the presence of the functional group for aluminum [33]. This confirms the successful formation of the γ-phase alumina. Additionally, bands observed in the FTIR spectra suggested that there were very few water molecules attached to the $Al(OH)_3$ [30]. Additionally, the band located at 500 cm^{-1}–800 cm^{-1} could be attributed to Al—O—H. The peaks for the —OH stretch were deducted at

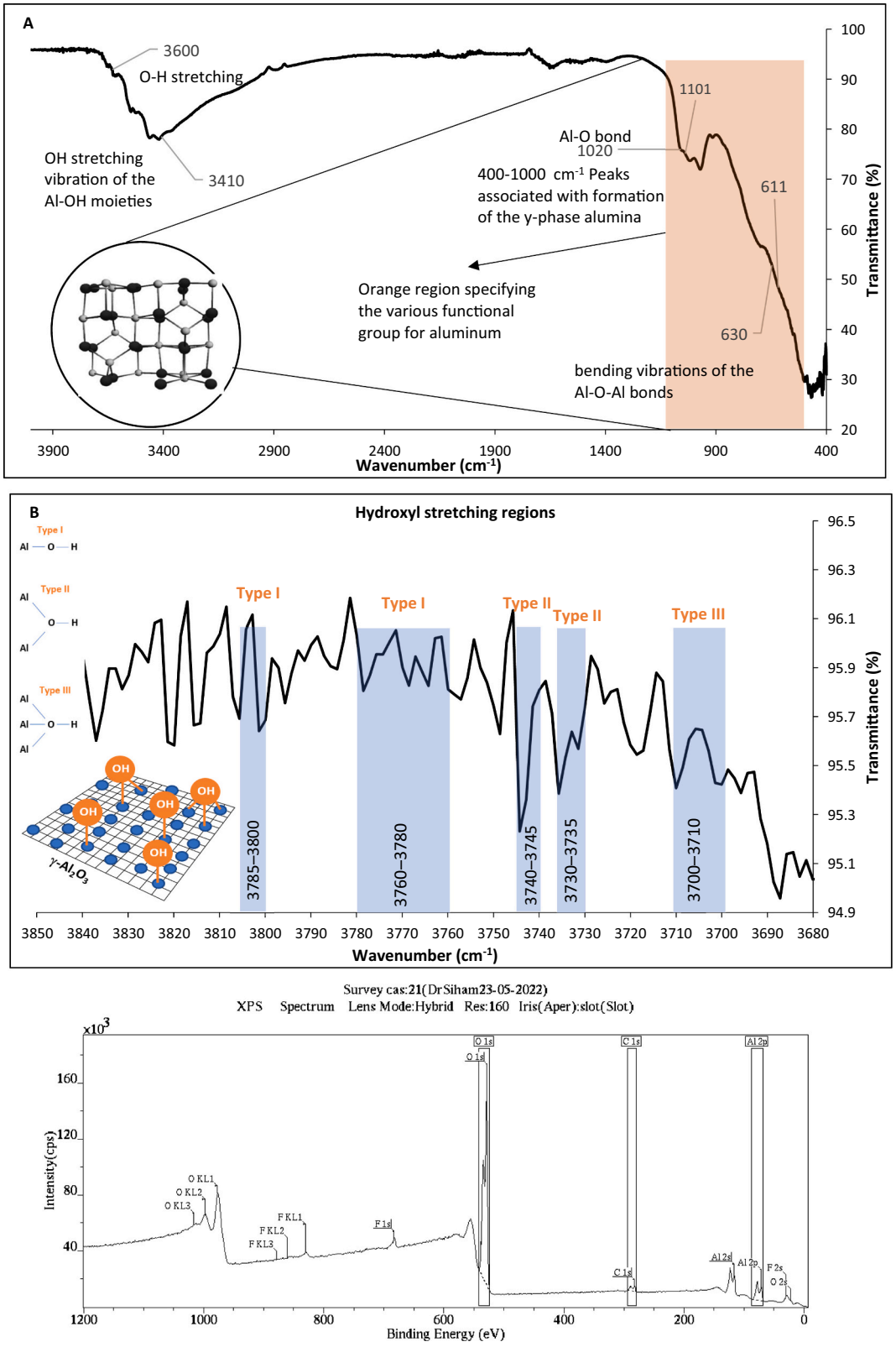

Fig. 3. FTIR spectra of nano-γ-Al_2O_3, A. 4000 cm^{-1}–400 cm^{-1}, B. 3850 cm^{-1}–3680 cm^{-1}, showing the types of OH-species on the surface of alumina and C. XPS spectrum of the prepared nano-γ-Al_2O_3 before adsorption.

3600 cm^{-1} which can be attributed to the aluminum (hydra) oxide minerals [34]. The peak that was observed between 3650 cm^{-1}–3120 cm^{-1} was due to the symmetrical and asymmetrical stretching of OH while the peak at 1630 cm^{-1}–1400 cm^{-1} was due to the bending of O—H bonds, present in water. Additionally, the prominent peak observed at 3410 cm^{-1} shows the presence of OH stretching vibration of the Al—OH moieties. While the bands between 1020 cm^{-1}–920 cm^{-1} were related to the Al—O bond [35]. Furthermore, the chemical state of the prepared

nano-γ-Al_2O_3 was further characterized by XPS as illustrated in Fig. 3C. Accordingly, the peak located at 74.4 eV in the XPS spectra is also attributed to Al—O bonding, while the peak at 70.5 eV indicated the presence of Al_2O_3 [19,36].

The FTIR graph for nano-γ-Al_2O_3 was further enhanced between the 3680–3850 cm^{-1} to understand the two main groups of surface hydroxyl groups (—OH), namely isolated hydroxyl groups with infrared peaks (>3600 cm^{-1}), and self-associated hydroxyl groups with infrared peaks (>3600 cm^{-1}). However, the OH groups could be coordinated to one, two, and three Al^{3+} in the surface layers (Onfroy et al., 2009), as shown in Fig. 3B. The intensity of the OH peaks refers to the density of OH groups present on the surface of the nano-γ-Al_2O_3. Accordingly, type III is the dominant coordination, then type II and type I. These findings were in line with Basu et al. [35] and Rabung et al. [37].

3.1.4. Thermal properties

Fig. 4 shows the TGA curve of the prepared nano-γ-Al_2O_3. Accordingly, the pattern of weight decrease with increasing temperature. Such observation was similar to the findings by Castillo et al. [38] and Asencios et al. [23]. TGA profile shows four distinct stages, as marked in Fig. 4. The first loss of around 7 % can be observed at around 28 °C to 50 °C, which can probably be due to the dehydration process and the desorption of the physisorbed water from the surface [39]. The second weight loss was observed at around 50 °C–170 °C. The third loss from 170 °C–240 °C, can be associated with rapid autoignition, which could be due to the quick evaluation of nitrogen dioxide. The exothermic peak recorded can be attributed to the combustion of organic compounds [39]. Hence, 300 °C was chosen to obtain nano-γ-Al_2O_3 nanoparticles. After the peak at 300 °C, the weight loss gradually slowed down, this can be due to the formation of nano-γ-Al_2O_3 [40]. The last stage showed an insignificant weight loss, which can be attributed to the dihydroxylation of nano-γ-Al_2O_3 and other alumina transitions that may have occurred. Overall, the total weight loss was 29 % showing nano-γ-Al_2O_3 is resistant to high temperatures.

3.2. Effect of the pH on the percentage removal

It is well established that boron, in aqueous solutions, exists as H_3BO_3 and $B(OH)_4^-$. The dominant existence of either boric acid or tetrahydroxyborate is dictated by the pH of the aqueous solution; with the presence of boric acid being dominant at lower and neutral pH, while tetrahydroxyborate occurrence is more in alkaline solution [5]. However, at a pH range between 7.2 and 11, both boric acid and tetrahydroxyborate exist in equilibrium. Since the pH plays a critical role in the adsorption at the water-absorbent interface, the optimization of the parameter was performed by investigating the boron removal percentage as a function of pH, as illustrated in Fig. 5. As seen, an increase in pH resulted in a higher percentage of boron removal. At lower pH, the electrostatic forces on the adsorbent and boric acid negatively affect the boron adsorption. It can be assumed that at lower pH boron was present in the solution in various forms including $B(OH)_3$, which under acidic conditions is mainly uncharged, consequently resulting in low boron adsorption in an acidic environment [2,14]. Likewise, at a pH of 10, the highest removal was reached. Bouguerra et al. [41] used activated alumina for the removal of boron and found pH higher than 9 showed high boron adsorption. Accordingly, Bouguerra et al. [41] explained that the boron species that are present in an aqueous solution are determined by the pH and the concentration of the solution. Usually, the point zero (pH_{PZC}) of alumina ranges between 8.7 and 9.0, while the pKa for boric acid is 9.2. Consequently, the surface of the prepared alumina was positively charged until $pH < pH_{PZC}$. Likewise, the same phenomenon can be used to explain the high adsorption of boron at pH 10. At pH 10, the anionic species would have a stronger interaction with the adsorbent and thus result in greater removal of the species. However, the optimal solution pH is also reliant on the surface chemistry of the adsorbent used [13]. Additionally, the adsorption of earth-alkaline metal ions on alumina increased as the pH of the solution increased. Furthermore, the affinity of the earth's alkaline metal towards hydrous γ-Alumina decreased as the ionic size of the ion increased [42].

While, on the other hand, the bromide ions' adsorption in an aqueous solution is also illustrated in Fig. 5. From Fig. 5, it can be observed that bromide preferred a weakly acidic environment, and the maximum adsorption efficiency was around 57 %, which was obtained at pH 6 using nano-γ-Al_2O_3. It can be seen from Fig. 5, the change in pH did not dramatically influence bromide adsorption. This is because bromide is very stable at different pH values [43]. The pH of the solution is very crucial as it also determines the surface charge of the adsorbent in the solution. At low pH, the surface of the adsorbent was positively charged, which caused the active sites on nano-γ-Al_2O_3 to be protonated. Additionally, the increase in hydrogen ions at low pH may also have been

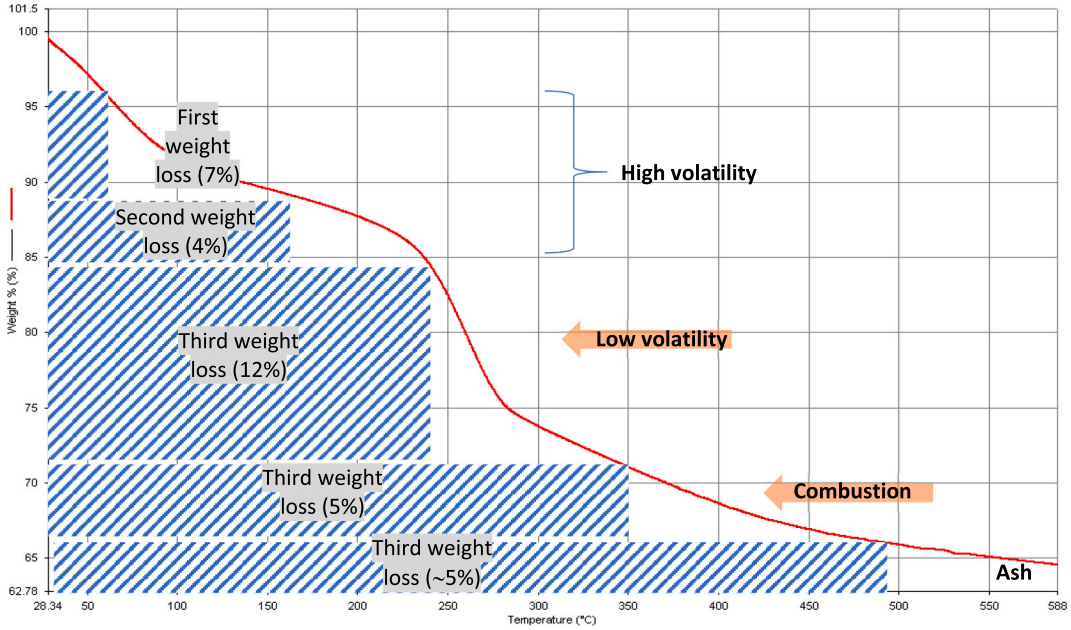

Fig. 4. TGA graph for nano-γ-Al_2O_3.

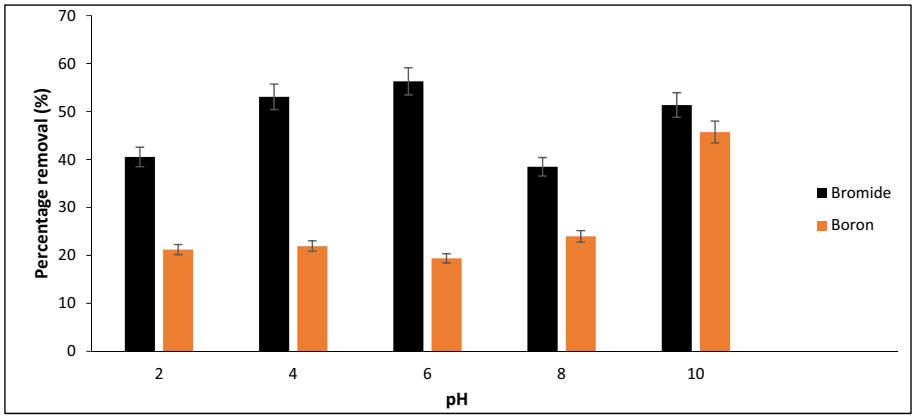

Fig. 5. Effect of pH on bromide and boron adsorption onto nano-γ-Al_2O_3. The experimental conditions were: Adsorbent dose, 0.05 g/50 mL, temperature 25, ignited at 165 rpm for 24 h.

attributed to the high bromide removal. When the pH was lower than 6 the removal of bromide was negatively affected. This may be due to several factors including electrostatic repulsion between bromide and the surface of the nano-γ-Al_2O_3. In general, in more acidic solutions, bromide adsorption occurs in a competitive process with the presence of hydrogen ions in the solution. Therefore, as the pH increased, bromide adsorption also increased this can be attributed to the surface of the adsorbent that was almost free of adsorbed hydrogen. It is worthy pointing out that in an acid medium bromide adsorption is stronger than in an alkaline medium. Additionally, the pH was adjusted by inducing 0.5 M of HCl; this may have caused competitive adsorption of chloride ions, which would have also influenced bromide adsorption to nano-γ-Al_2O_3 to some extent. While adjusting pH 6 required a very minimum amount of hydrochloric [44]. Lastly, under alkaline conditions, there would be hydroxyl ions competition. However, at pH 10, 51.35 % of bromide was removed; this could be accounted for as a faked adsorption behavior phenomenon [45]. Additionally, it is also possible that at high pH, the bromide structural transition takes place, which can cause bromide to change its form to other components. Thus, the increase of bromide ions at high pH was observed which might not be of pure bromide but perhaps of a compound such as bromate (BrO_3^-), thus, the adsorption of bromide will be more suitable under neutral or weakly acidic conditions [46].

3.3. Effect of concentration of boron and bromide on nano-γ-Al_2O_3

Fig. 6 shows how the adsorption performance of boron and bromide onto nano-γ-Al_2O_3 changed as the initial concentration (C_e) increased. The percentage removal was investigated under an initial concentration of 10 mg/L to 100 mg/L of boron and bromide solutions. It was observed that as the initial concentration increased, the percentage removal of boron and bromide also increased simultaneously. The amount of the boron and bromide ions adsorbed on the adsorbent is a function of concentration at equilibrium. Thus, by increasing the initial boron and bromide concentrations, it was observed that the adsorption of boron and bromide increased onto the nano-γ-Al_2O_3 surface, as indicated by the trend line in Fig. 6. This is also predictable as it suggests the mass transfer of boron and bromide ions to the available adsorption sites on nano-γ-Al_2O_3. Boron adsorption increased from 65.55 % to 75.55 % as the concentration increased from 10 mg/L to 30 mg/L, respectively. The percentage removal for boron continued to increase as the initial concentration of boron increased. The maximum percentage removal of boron reached 88.35 % at 100 mg/L on nano-γ-Al_2O_3. It can be assumed that the increase of boron ions in the initial concentration in the solution caused a stronger driving force that is greater than the mass transfer resistance [47]. Furthermore, it can also be assumed that the adsorption process did not reach equilibrium. Similar results have been also reported by Wang et al. [6] while investigating boron adsorption

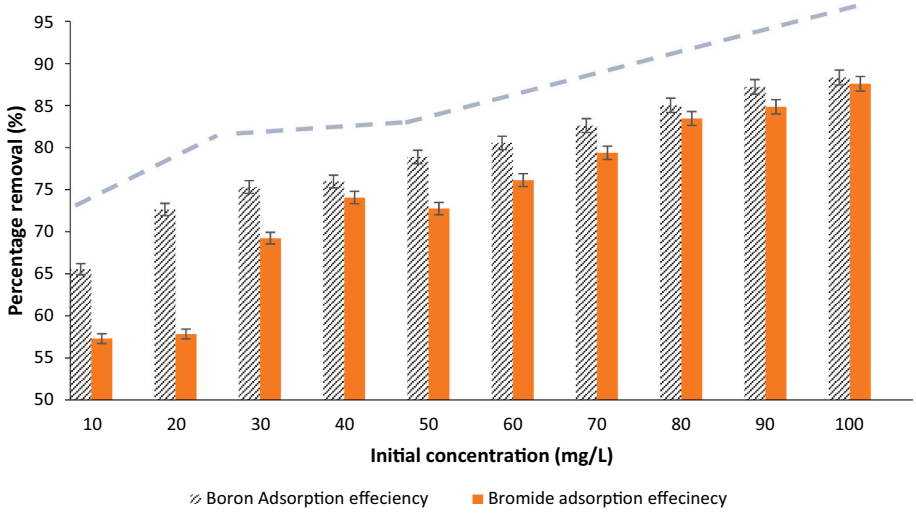

Fig. 6. The effect of initial concentration on the removal of boron and bromide. The experimental conditions were: Adsorbent dose, 0.05 g/50 mL temperature 25 °C, ignited at 165 rpm for 24 h.

efficiency onto graphene oxide composite (UIO-66-NH_2/GO). On the other hand, bromide adsorption also showed a similar trend. As the initial concentration increased from 10 mg/L to 40 mg/L, the percentage removal increased from 57.3 % to 74.06 %, respectively. At 100 mg/L, the percentage removal reduced slightly from 74.06 % to 72.75 %, and then gradually improved to 87.56 %. Similar to boron, it can be assumed that the adsorption process did not reach equilibrium. The high adsorption of both boron and bromide can be attributed to various reasons. For instance, the active sites on the surface of nano-γ-Al_2O_3 consist of a large surface area and good porosity are the two essential properties that favor adsorption. Additionally, the micropores' nature and structure, the surface morphology of the prepared nano-γ-Al_2O_3, and the active adsorption sites on nano-γ-Al_2O_3, are attributed to the capturing of boron and bromide ions [44]. Table 1 mentions various studies that have been conducted to remove boron and bromide from an aqueous solution.

3.4. Isotherm studies

3.4.1. Boron adsorption

Langmuir isotherm implies that the adsorption took place on a monolayer. The correlation coefficient (R^2) for boron adsorption was close to one (0.9800) as tabulated in Table 2. This indicates that boron adsorption onto nano-γ-Al_2O_3 could be explained by the Langmuir model. The separation factor (R_L) was close to 1 (0.89–0.93), which showed that the adsorbent was favorable energetically. The affinity between the adsorbate and adsorbent, which is denoted by K_L indicated a strong binding between boron ions and nano-γ-Al_2O_3 at 35 °C. When the temperature increased to 35 °C, the maximum adsorption capacity (Q^o_{max}) increased, however, (Q^o_{max}) decreased when the temperature further increased to 45 °C. Boron adsorption onto nano-γ-Al_2O_3 could be best explained by Langmuir isotherm as the R^2 is 0.98 and Chi-square $(\chi)^2$ 15.07 at 25 °C. While Freundlich isotherm implies that a heterogeneous surface was involved in the adsorption, and the distribution of heat is non-uniform throughout the surface. Similarly, the R^2 for boron adsorption was between 0.7200 and 0.9000, while the K_f value showed an increase from 13.48 (mg/g)(mg/L)^n to 109.18 (mg/g)(mg/L)^n at 25 °C and 35 °C, respectively and then a decrease from 45 °C to 105.32 (mg/g)(mg/L)^n this indicated that up to 35 °C the adsorption capacity continued to increase. The *n* value indicates if the reaction was physical adsorption or chemical adsorption. If the *n* value is <1 it indicates that the reaction was chemical adsorption while if the value is higher than 1, the reaction was physical adsorption. Accordingly, from the data in Table 2 it can be seen that at 25 °C and 35 °C, the adsorption was chemical adsorption, while at 45 °C the adsorption changed to a physical process. The reaction was favorable at 35 °C and 45 °C, as indicated by the $\frac{1}{n}$ values (5.860 and 0.6900, respectively). The heat adsorption constant that is denoted by b_T revealed that at 35 °C and 45 °C, the heat adsorption was high, 53.40 J/mol and 44.62 J/mol, respectively. The equilibrium-binding constant (A_T) for Temkin isotherm, presented a gradual increase as the temperature increased. For instance, at 25 °C the A_T value was 3.79 L/g, which gradually increased to 5.960 L/g at 35 °C and 6.530 L/g at 45 °C, respectively. Finally, the Dubinin-Radushkevich adsorption model was found not to be suitable for both boron and bromide as the R^2 values were between 0.5300 and 0.7600.

3.4.2. Bromide adsorption

The correlation coefficient (R^2) for bromide adsorption, on the other hand, was likewise close to 1 (0.9800–0.9900). This suggests that the Langmuir isotherm could also explain bromide adsorption onto nano-γ-Al_2O_3. The R_L was found to be more than one, indicating that the adsorption was energetically advantageous (0.90–0.98). The *b* showed that there was a strong binding between boron ions and nano-γ-Al_2O_3 at 25 °C, which was 59.90. It is noteworthy to mention that the Q^o_{max} was 90.72 at 25 °C and gradually decreased as the temperature increased. Likewise for bromide adsorption onto nano-γ-Al_2O_3, it can also be said that the adsorption process was best explained using the Langmuir model at 25 °C as the R^2 is 0.99 and Chi-square $(\chi)^2$ 6.987 with maximum adsorption capacity being 90.72 mg/g. While for Freundlich isotherm, the R^2 for bromide adsorption was between 0.82 and 0.85, while the K_f value increased generally as the temperature increased, from 25 °C to 45 °C. The value decreased from 4.520 mg/g to 1.080 mg/g at 25 °C and 35 °C, respectively, and then slightly increased to 2.930 mg/g at 45 °C. The value suggested that the adsorption of bromide was chemical adsorption at 25 °C as the value is <1, however, as the temperature increased there to 35 °C and 45 °C the adsorption process followed physical adsorption, as seen from *n* value which increased to 3.410 and 1.096 at 35 °C and 45 °C, respectively. The $\frac{1}{n}$ value exhibited the process was favorable. The A_T showed a general decline as the temperature increased. For instance, at 25 °C A_T value was 4.650 L/g, which gradually decreased to 2.940 L/g and 45 °C. The b_T value revealed that at high temperatures the heat adsorption was high, (35°C, 66.61 J/mol) and (45°C, 104.45 J/mol). The results were similar to Pouya et al. [55] who studied the adsorption of Pb(II) on γ-Al_2O_3, Banerjee et al. [32] utilized alumina nanoparticles for the removal of a hazardous dye, and Asencios et al. [23] who synthesized alumina for the adsorption of Pb, Cd, and Zn.

3.5. Effect of temperature

Temperature effects on boron and bromide adsorption onto nano-γ-Al_2O_3 were also examined. The trend of this parameter is illustrated in Fig. 7. It is evident that both boron and bromide favored low temperatures (25 °C) and resulted in a high removal capacity of 88.35 % and 87.65 %, respectively. This finding is very noteworthy, as it indicates adsorption of boron and bromide on nano-γ-Al_2O_3 does not require high temperature, which indicates cost-effectiveness and a more sustainable option.

Table 1
Compilation of various studies that have reported the removal efficiency/maximum capacity of boron and bromide using various adsorbents.

Method	Removal	Optimum pH	Adsorption capacity (mg.g)	Dosage (g)	Element	Reference
Activated carbon	50–60 %	9.26	0.950–1.680	1.000	Boron	[48]
Fly ash	90 %	NR	NR	1.000	Boron	[49]
Eggshell wastes	96.3 %	6	25.99–86.20	0.050	Boron	[13]
Waste tire rubber	76.7 %	2	1.06–3.27	0.050	Boron	[50]
Activated Alumina	40–65 %	8–8.5	NR	0.050	Boron	[51]
Polymer grafting polyol compounds	NR	9	2.540	0.010	Boron	[52]
Fibrous polymeric chelator containing glycidol moiety	NR	7	25.9	0.5	Boron	[53]
Cellulose-based beads modified with TEMPO-mediate	82.33	10	0.5524–1.165	0.050	Bromide	[46]
Silver-loaded porous carbon spheres	94 %	5	1.20	0.008	Bromide	[44]
Natural pumice and aluminum-coated pumice	58–72 mg/g	8	58.82–76.92	8.000	Ethidium bromide	[54]
Nano-γ-Al_2O_3	88.35 %	6	16.21–25.86	0.005	Boron	Current study
Nano-γ-Al_2O_3	87.65 %	10	19.09–90.72	0.005	Bromide	Current study

Table 2
Isotherm parameter for boron and bromide adsorption onto nano-γ-Al_2O_3.

Boron										
Langmuir						Freundlich				
Temperature (°C)	Q^o_{max} (mg/g)	K_d	*b* (L/mg)	R^2	χ^2	K_f (mg/g)(L/g)$^{1/n}$	n	1/n	R^2	χ^2
25	16.21	10.58	11.64	0.9800	15.07	13.48	−0.3100	−3.200	0.8200	50.31
35	25.86	35.66	36.70	0.9700	7.94	109.18	0.1700	5.860	0.7700	43.73
45	19.65	31.27	32.31	0.9700	17.58	105.319	1.442	0.6900	0.9000	95.3

Boron										
Dubinin-Radushkevich						Temkin				
Temperature (°C)	q_s (mg/g)	K_{ad} (mol^2/kJ^2)	E (kJ/mol) (=1/(2K_{ad})$^{0.5}$)	R^2	χ^2	B (J/mol)	b_t	A_T (L/g)	R^2	χ^2
25	93.00	6×10^{-04}	28.90	0.8600	25.02	53.22	42.64	3.790	0.660	441.2
35	42.14	5.9×10^{-03}	9.210	0.6700	0.099	47.97	53.40	5.960	0.810	196.7
45	32.56	6.9×10^{-03}	8.510	0.9500	918.7	59.26	44.62	6.530	0.760	6063

Bromide										
Langmuir						Freundlich				
Temperature (°C)	Q^o_{max} (mg/g)	K_d	*b* (L/mg)	R^2	χ^2	K_f (mg/g)(L/g)$^{1/n}$	n	1/n	R^2	χ^2
25	90.72	18.85	59.90	0.9900	6.987	4.527	0.4700	2.108	0.8200	10.44
35	30.89	29.78	30.81	0.9800	2.233	1.080	3.410	0.2900	0.8000	1345
45	19.09	55.00	16.01	0.9900	8.809	2.910	1.096	9.120	0.8500	32.66

Bromide										
Dubinin-Radushkevich						Temkin				
Temperature (°C)	q_s (mg/g)	K_{ad} (mol^2/kJ^2)	E (kJ/mol) (=1/(2K_{ad})$^{0.5}$)	R^2	χ^2	B (J/mol)	b_t	A_T (L/g)	R^2	χ^2
25	68.48	1×10^{-05}	224.0	0.8300	47.45	53.12	42.72	4.650	0.5200	9769
35	61.35	9×10^{-06}	23.00	0.8500	7.997	38.45	66.61	4.910	0.6100	447.5
45	53.222	5×10^{-06}	316.0	0.8200	5.894	25.32	104.5	2.940	0.7100	32.60

3.6. Thermodynamic studies

The thermodynamic behavior of boron and bromide adsorption was investigated by determining thermodynamic parameters such as Gibbs free energy (ΔG°), enthalpy (ΔH°), and entropy (ΔS°), as shown in Table 3. From the data obtained, boron adsorption was spontaneous and feasible as suggested by the negative value of ΔG ° . The value estimated for ΔG° were − 5574 kJ/mol, −9230 kJ/mol, and − 9193 kJ/mol at 25 °C, 35 °C, and 45 °C, respectively; demonstrating that adsorption was more favorable at low temperatures. The enthalpy value (ΔH °) was positive which signified that the process followed an endothermic reaction, while the negative value of entropy suggested that throughout the process the adsorbate concentration increased on the solid adsorbent surface which lead to a decrease in randomness at a solid-liquid interface. On the other hand, the thermodynamic parameter revealed that the adsorption of bromide followed an exothermic reaction, as the ΔH° value was negative (−0.502 kJ/mol). Similar to boron, as temperature increased, the value of ΔG° decreased from −8782 kJ/mol to −9413 kJ/mol at 298 °C and 318 °C, this observation was in accordance with the adsorption capacities which showed the adsorption efficiency decreased with the increase in temperature. Lastly, bromide adsorption had a good affinity at the solid-liquid surface as indicated by the positive value of ΔS°(165.4 J/mol.K). Similar findings were reported by Banerjee et al., [32] in their study on removing hazardous dyes using alumina.

3.7. Adsorption kinetics studies

The adsorption kinetic models are used to empirically predict the mechanism controlling the adsorption of bromide and boron [57]. The pseudo-first-order and pseudo-second-order were applied to describe the kinetic process of the bromide and boron adsorption onto the nano-γ-Al_2O_3. The parameters of both models for bromide and boron are tabulated in Table 4. Pseudo models assume that the reaction was a pseudo-chemical reaction process. The data were plotted to the pseudo-first and second other equation to have a further clearer understanding of bromide and boron adsorption onto nano-γ-Al_2O_3. Accordingly, if a reaction follows a pseudo-first-order it will obtain a straight line when ln (q_t-q_e) is plotted against time *t*, while in pseudo-second-order the straight line is obtained when the $\frac{t}{q}$ is plotted against time. From Fig. 8 A and B boron adsorption onto nano-γ-Al_2O_3 obeyed the pseudo-second-order with a very high R^2 value (0.99) while for the pseudo-first-order the R^2 value was 0.08. In addition, the q_e value obtained in pseudo-second-order is in agreement with the calculated amount. Furthermore, K_1 indicates the reaction rate per minute the value shows the reaction was comparatively faster 1.64 while the maximum concentration was 527 mg/g. This indicates that covalent bonding or perhaps electron transfer between the various functional groups present on nano-γ-Al_2O_3 were involved in capturing boron ions. This finding is in line with the earlier findings of the functional groups and elemental composition of the adsorbent that was deducted from the surface of the adsorbent. Furthermore, the reaction is likely to be affected by chemical adsorption [58]. Wang et al. [59] studied the adsorption of boron onto UiO-66-NH_2/GO and obtained similar results, additionally, they also mentioned that other forces such as electrostatic attraction were also involved in the successful adsorption of boron.

On the other hand, bromide adsorption onto nano-γ-Al_2O_3 can be

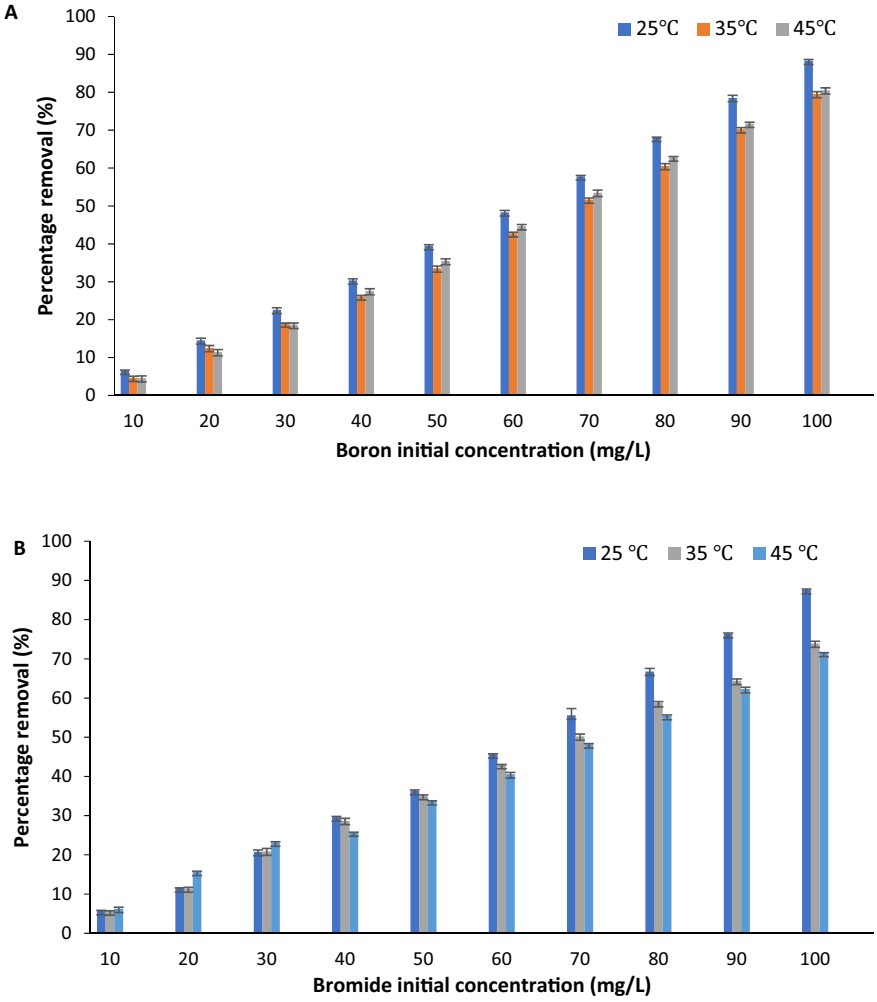

Fig. 7. Effect of temperature on the percentage removal of (A) boron and (B) bromide on nano-γ-Al_2O_3. The experimental conditions were adsorbent dose 0.05 g in 50 mL, temperature 25 °C, 35 °C, and 45 °C, at 165 rpm for 24 h.

Table 3
Thermodynamics properties of Boron and bromide adsorption onto nano-γ-Al_2O_3.

Temperature (°C)	ΔG° (kJ/mol)	ΔH°(kJ/mol)	ΔS°(J/mol.K)
Boron			
25	−5574		
35	−9230	20.03	−5202
45	−9193		
Bromide			
25	−8782		
35	−10,690	−0.502	165.4
45	−9413		

Table 4
Kinetic parameter of boron and bromide adsorption onto nano-γ-Al_2O_3.

Bromide			Boron		
Model	Parameter	Value	Model	Parameter	Value
Pseudo first law	K_1 (1/min)	2.67 × 10^{-4}	Pseudo first law	K_1 (1/min)	1.64
	q_e (mg/g)	572		q_e (mg/g)	527
	R^2	0.51		R^2	0.08
Pseudo second law	K_2 (g/mg.min)	2.45	Pseudo second law	K_2 (g/mg.min)	2.53 × 10^{-4}
	q_e (mg/g)	322		q_e (mg/g)	769.23
	R^2	0.98		R^2	0.99
Intra-particle diffusion model	k_{id} (mg/g.$min^{0.5}$)	6.44	Intra-particle diffusion model	k_{id} (mg/g.$min^{0.5}$)	2.69
	B	224.9		B	216.8
	R^2	0.95		R^2	0.94

seen to follow the pseudo-second-order; with R^2 being 0.98 while for the pseudo-first-order it was 0.51, indicating that the reaction was governed by chemical exchange through electron sharing. The K_2 value for bromide was 2.45 g/mg.min, which shows the reaction for bromide was much faster than for boron. This indicates that the adsorption occurred on a heterogeneous surface [60]. Which agree with earlier finding, where SEM and TEM revealed that the surface of the prepared adsorbent was covered with different sizes of pores and cavities Furthermore, it also implies, that bromide fixation onto nano-γ-Al_2O_3 was mainly due to chemo-sorption, which was due to several forces including electron exchange between the ions and the adsorbent [61]. Jiang et al. [62] in their study for the removal of bromide using electrochemically induced dual-site adsorption composite film of Ni-MOF derivative/NiCo LDH.

The failure of the pseudo-first-order in correlating adsorption kinetic experimental data is usually due to theoretical interpretations of this equation. In pseudo-first-order, it is commonly assumed that the total sorption process is controlled by the rate of adsorption/desorption processes, which is perceived as a chemical reaction on the adsorbent's surface. However, in many circumstances, the rate of solute diffusion

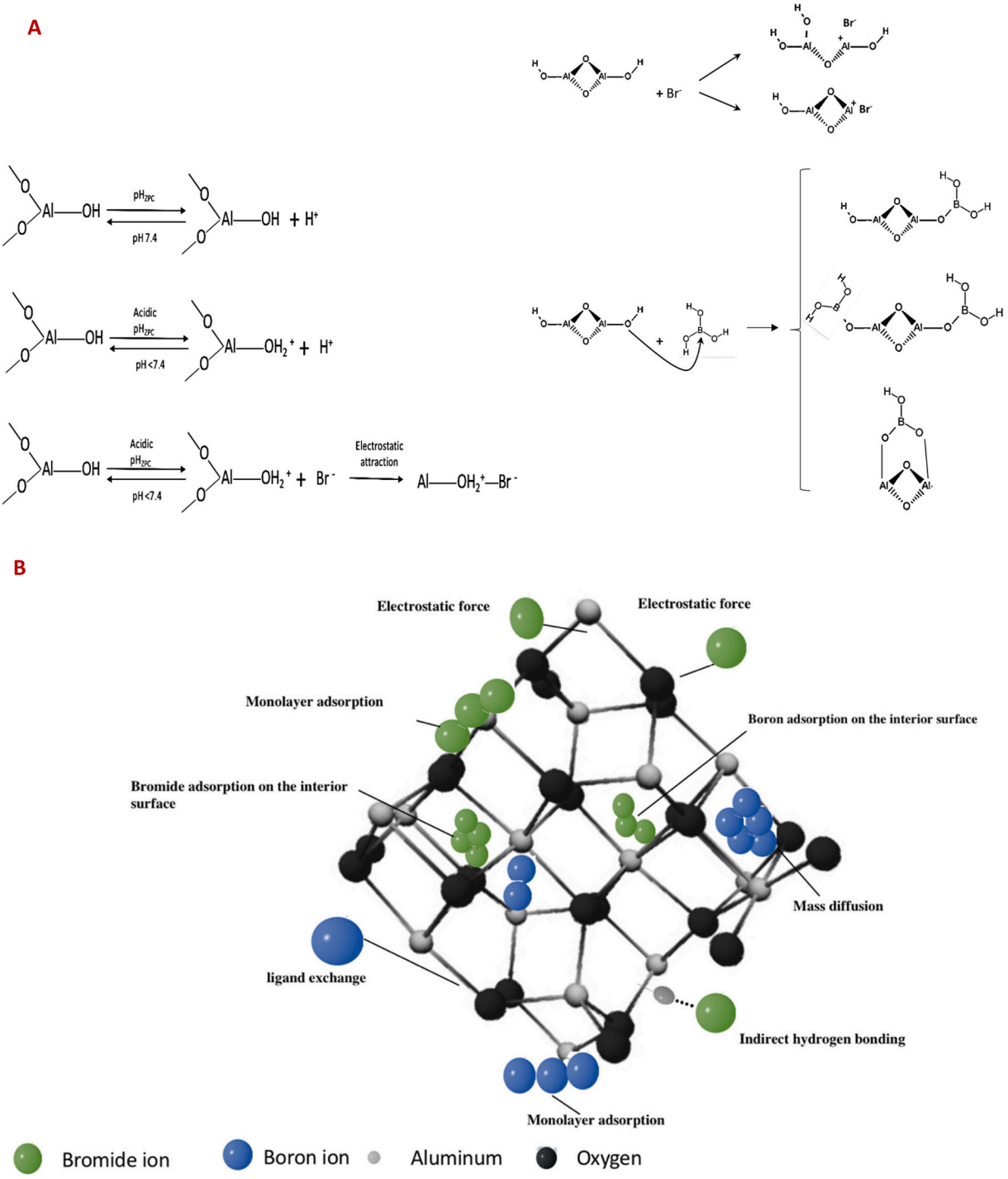

Fig. 8. (A) Illustration of chemical reaction involved during bromide adsorption on nano-γ-Al_2O_3 (modified from Banerjee et al.[32]) and (B) illustration of various mechanisms involved in both boron (blue) and bromide (green) adsorption. (For interpretation of the references to colour in this figure legend, the reader is referred to the web version of this article.)

into the interior of the adsorbent also determines the adsorption mechanism, and the pseudo-first-order model does not account for this phenomenon [63]. Lastly, the data was also compared using the intra-particle diffusion model and for both the bromide and boron model the value on both graphs the line could not pass through the origin of the graph, indicating that the intraparticle diffusion was not the only force involved in the process. In addition, from Table 4, the intercept value (*B*) for bromide was 224.9 and for boron was 216.8, which further confirmed that the intra-particle diffusion was not the dominant mechanism governing the adsorption of bromide and boron [63]. In addition, the rate constant was observed to be higher for bromide (6.44 mg/g.$min^{0.5}$) than boron (2.69 mg/g.$min^{0.5}$), this indicates that bromide adsorption onto the adsorbent was faster than boron. When comparing the thermodynamic studies result, at 25 °C for both boron and bromide the *n* value (Freundlich constant) was <1 which also indicated that the adsorption followed a chemo-adsorption.

3.8. Statistical analysis

The data for the influence of three different parameters, i.e. pH,

temperature, and concentration were validated using two-way NOVA. The data is tabulated in Table 5. For both reactions, the probability value (p-value) was <0.05 for boron, which was 7.39×10^{-30} while for bromide it was 2.46×10^{-35}, suggesting that the data was significantly different between groups. While the F-value was greater than F-crits, for boron F value was 477.0 and for bromide 111.0 while the F-crits was 2.210 and 2.290, respectively this showed adsorption of boron and bromide ions were significantly affected by the initial concentration of boron and bromide and temperature.

Similarly, boron adsorption was significantly affected by the change in pH, as the p-value (2.32×10^{-8}) was <0.050 and the F value was higher than F-crits 78.40 and 3.210, respectively. However, bromide adsorption was not significantly affected by the change in pH as the p-value was higher than 0.05 (0.55).

3.9. Adsorption mechanism

During the adsorption process, more than one mechanism is present that controls the adsorption process, while the model can express the adsorption pathway but are unable to express the precise adsorption mechanisms involved during the process. Fig. 8B shows a combined schematic representation of the boron and bromide adsorption mechanism onto nano-γ-Al_2O_3 that would have occurred during the respective adsorption. In general, both interior and exterior adsorption of boron and bromide would have occurred on nano-γ-Al_2O_3. The adsorption mechanism, on the other hand, can be assumed to be based on the surface chemistry of the nano-γ-Al_2O_3. The presence of metal oxides in nano-γ-Al_2O_3 causes hydroxylation of the metal oxide surface in the aqueous phase. As a result, the metal oxide might act amphoterically under the effect of different pH values [56]. The aqueous pH condition has a significant influence on the surface characteristics of alumina nanoparticles. Fig. 8A illustrates the possible mechanisms that may have taken place for bromide adsorption. The net surface charge at pH 7.4 is near zero, and the system becomes electrostatically neutral. While in an acidic medium, principally the surface is positively charged, which electrostatically attracts the bromide ions, which will ultimately lead to high adsorption as shown in reaction (3) [32]. Thus, it can be deduced that electrostatic attraction between the electronegative bromide and the positively charged nano-γ-Al_2O_3 majorly contributed to the high efficiency of bromide adsorption [64]. Furthermore, aluminum atoms exhibit strong Lewis acidity and have an electronegativity of 1.5 while bromide has an electronegativity of 2.8, resulting in a 1.3 electronegativity difference for the aluminum and bromide bond. Thus, it can be also deduced there was a strong electronegativity attraction and polar covalent bond.

While the mechanism of boron onto nano-γ-Al_2O_3 can be assumed as a ligand exchange with the reactive hydroxyl groups that are found on the surface of nano-γ-Al_2O_3. The shift of pH of the point zero of charge (pH_{ZPC}) present on the mineral when the adsorbent becomes specially adsorbed on the mineral surface is often characterized as ligand exchange [65]. Additionally, from the results obtained it can also be deduced that the occurrence of film diffusion can also be another adsorption mechanism where the cations' movement from the bulk solution to the nano-γ-Al_2O_3 external surface occurred. Lastly, the increase in pH could be inferred that $B(OH)_4^-$ species such as $B(OH)_3$, or $B(OH)_4^-$ could form trigonal and tetrahedral boron species to be adsorbed on the surface of nano-γ-Al_2O_3. Similar findings were also reported by Al-Ghouti & Salih. [65].

Table 5
Analysis of Variance for the effect of temperature and pH on boron and bromide adsorption onto nano-γ-Al_2O_3.

Condition	p-Value	*F value*	F-crits
Temperature Boron	7.39×10^{-30}	477.0	2.210
pH Boron	2.32×10^{-8}	78.40	3.210
Temperature Bromide	2.46×10^{-35}	111.0	2.290
pH Bromide	0.5500	80.40	4.450

3.10. Desorption studies of nano-γ-Al_2O_3

In any adsorption water treatment, it is crucial to consider the regeneration step. The effectiveness of any adsorption process is primarily determined by its expenses as well as the amount of solid waste produced. This could be minimized if the used adsorbent can be recycled multiple times easily and effectively. The regeneration of nano-γ-Al_2O_3 was performed by washing the spent adsorbent (boron or bromide loaded nano-γ-Al_2O_3) with two different desorption agents 0.5 M and 1 M of hydrochloric acid (HCl). HCl was preferred over other acids to avoid the interference of other anions. Results indicated that 0.1 M of HCl was able to remove 89.6 % of boron and 91.6 % of bromide. This could be due to the Lewis acid-base reaction as discussed earlier. These results demonstrated the strong feasibility of nano-γ-Al_2O_3 regeneration.

3.11. Reusability of the spent adsorbent

Determining the possibility of reusing an adsorbent is very crucial as it aids in reducing the cost, helps preserve the environment, and proves to be a sustainable option. Thus, this study also performed the reusability of the spent adsorbent to explore the efficiency of the prepared adsorbent. The removal percentage for boron and bromide was calculated through four and five adsorption-desorption cycles until it reached 50 % percentage removal. For boron, it was found that the first cycle had 89.32 % percentage removal followed by 75.24 %, and 67.43 % and the forth cycle reported 54.32 % boron removal while for bromide it was found that the first cycle was able to remove 91.23 % of bromide, followed by 84.24 %, 73.45 %, 66.73 %, and the fifth cycle was removed 49.33 %. In general, it was observed with an increase in the number of cycles the ability of the adsorbent to remove boron or bromide also decreased gradually. The decrease in the nano-γ-Al_2O_3 adsorption performance can be due to the reduction of sites available on the nano-γ-Al_2O_3 surface, and the loss of adsorbents after each reuse cycle.

3.12. Application of nano-γ-Al_2O_3 to real wastewater sample

The feasibility and efficiency of nano-γ-Al_2O_3 were also evaluated by using real groundwater, which was collected from a local area. The methodology and the complete characterization are mentioned in one of our preliminary research (Ahmad et al. 2022). The collected groundwater pH level was between 6.89 and 7.94, while the total dissolved solids (TDS) and conductivity were 598.87 mg/L–156,433 mg/L and 0.92 μS/cm–22.33 μS/cm, respectively. Additionally, the groundwater is laden with various cations and anions. Accordingly, bromide's initial concentration was found to be 21.98 mg/L, and boron's initial concentration was found to be 16.02 mg/L. After adsorption, the IC results indicated no traces of bromide, proving that bromide was 100 % successfully adsorbed. On the other hand, 96.25 % of boron was successfully adsorbed. Surprisingly the prepared nano-γ-Al_2O_3 was also able to adsorb sulfate substantially. The initial concentration was found to be 11,543 mg/L in the groundwater, while after adsorption the sulfate concentration was reduced by 99 %. Indicating that the prepared nano-γ-Al_2O_3 adsorbent can adsorb multiple ions in one run. Proving that the adsorbent is environmentally and economically very feasible.

3.13. Cost analysis

Cost analysis is also another crucial parameter that should be considered for any potential adsorbent. In this study, aluminum foil was collected as a waste source, making the raw material price insignificant. Based on the solutions and other overhead costs required in this study, the total cost to prepare 5 g of nano-γ-Al_2O_3 was 0.85 United States Dollars (USD$). This is very minimal in contrast to Bai et al. [60], who in

their study reported that the synthesis of T-resin was 13.02 USD$ (87.19 CNY/kg) which was prepared for boron removal. While commercial activated alumina can cost between 1.5 and 3.5USD$/kg [67].

4. Conclusion

In this study, nano-γ-Al_2O_3 was successfully prepared from waste aluminum foil. This study may be regarded as one of its kind as for the first time nano-γ-Al_2O_3 was used to effectively remove boron and bromide from an aqueous solution. The stable structure nano-γ-Al_2O_3 and the presence of various functional groups were found to be favorable for boron and bromide ion entry into the exterior and interior surface matrix of nano-γ-Al_2O_3. Several influencing factors such as pH, temperature, and concentration were studied. This study revealed that both ions react differently in an aqueous solution. Boron preferred a basic medium (pH 10) for its effective removal from nano-γ-Al_2O_3, while bromide preferred a less acidic environment (pH 6). The highest boron adsorption capacity was 25.86 mg/g, while the maximum bromide adsorption capacity was 90.72 mg/g. Isotherm studies showed that the adsorption process for both boron and bromide was best explained by the Langmuir model, for boron at 35 °C the maximum adsorption capacity was recorded while bromide preferred a low temperature and yielded a high adsorption capacity of 25 °C. The evaluated thermodynamic parameters revealed that boron followed an endothermic reaction while bromide followed an exothermic reaction. ΔG° value for both ions indicated that adsorption was favorable. Kinetic studies showed that pseudo-second-order could better explain the kinetics aspect of boron and bromide adsorption. The results from desorption experiments were >85 % indicating that the used adsorbent can be effectively reused. Hydrogen bonds, electrostatic attraction, and ligand bonds were some of the forces that were involved in the adsorption mechanism. It was also assumed that the adsorption occurred on both the interior and exterior surfaces of the adsorbent.

Declaration of competing interest

The authors declare that they have no known competing financial interests or personal relationships that could have appeared to influence the work reported in this paper.

Data availability

No data was used for the research described in the article.

Acknowledgment

This report was made possible by UREP grant # (26-076-1-008) from the Qatar national research fund (a member of Qatar Foundation). The statements made herein are solely the responsibility of the author(s). The FTIR, ICP, SEM, TEM, and IC analyses were accomplished in the Central Laboratories unit, Qatar University.

Appendix A. Supplementary data

Supplementary data to this article can be found online at https://doi.org/10.1016/j.jwpe.2022.103312.

References

[1] B. Gao, H. Yu, J. Gao, L. Liu, Q. Wang, C. Zhu, W. Wu, Occurrence and health risk assessment of trace metals in desalinated seawater using two desalination technologies, Pol. J. Environ. Stud. 29 (5) (2020).
[2] Z. Wang, Y. Jia, W. Song, X. Li, K. Xu, Z. Wang, Optimization of boron adsorption from desalinated seawater onto UiO-66-NH2/GO composite adsorbent using response surface methodology, J. Clean. Prod. 300 (2021), 126974.
[3] N. Kabay, M. Bryjak, N. Hilal (Eds.), Boron Separation Processes, Elsevier, 2015.
[4] WHO, Geneva, in: Boron. Environmental Health Criteria 204, World Health Organization, 1998.
[5] J. Kluczka, W. Pudło, K. Krukiewicz, Boron adsorption removal by commercial and modified activated carbons, Chem. Eng. Res. Des. 147 (2019) 30–42.
[6] M. Rahman, M.A.N. Tushar, A. Zahid, K.M.U. Ahmed, M.A.M. Siddique, M. G. Mustafa, Spatiotemporal distribution of boron in the groundwater and human health risk assessment from the coastal region of Bangladesh, Environ. Sci. Pollut. Res. 28 (17) (2021) 21964–21977.
[7] Z. Wang, Y. Jia, W. Song, X. Li, K. Xu, Z. Wang, Optimization of boron adsorption from desalinated seawater onto UiO-66-NH2/GO composite adsorbent using response surface methodology, J. Clean. Prod. 300 (2021), 126974.
[8] A. Hussain, R. Sharma, J. Minier-Matar, Z. Hirani, S. Adham, Application of emerging ion exchange resin for boron removal from saline groundwater, J. Water Process Eng. 32 (2019), 100906.
[9] M. Ateia, C.U. Erdem, M.S. Ersan, M. Ceccato, T. Karanfil, Selective removal of bromide and iodide from natural waters using a novel AgCl-SPAC composite at environmentally relevant conditions, Water Res. 156 (2019) 168–178.
[10] B. Wang, X. Guo, P. Bai, Colloids and surfaces a: physicochemical and engineering aspects removal technology of boron dissolved in aqueous solutions – a review, Colloids Surf. A Physicochem. Eng. Asp. 444 (2014) 338–344.
[11] WHO, in: Guidelines for Drinking-water Quality 216, World Health Organization, 2011, pp. 303–304.
[12] Izaak Cohen, Barak Shapira, Eran Avraham, Abraham Soffer, Doron Aurbach, Bromide ions specific removal and recovery by electrochemical desalination, Environ. Sci. Technol. 52 (11) (2018) 6275–6281.
[13] M.A. Al-Ghouti, M. Khan, Eggshell membrane as a novel bio sorbent for remediation of boron from desalinated water, J. Environ. Manag. 207 (2018) 405–416.
[14] M. Cai, W. Liu, W. Sun, Formation and speciation of disinfection byproducts in desalinated seawater blended with treated drinking water during chlorination, Desalination 437 (2018) 7–14.
[15] F. Valero, A. Barceló, R. Arbós, Electrodialysis technology: theory and applications, Desalination Trends Technol. 28 (2011) 3–20.
[16] M. Chen, O. Dollar, K. Shafer-Peltier, S. Randtke, S. Waseem, E. Peltier, Boron removal by electrocoagulation: removal mechanism, adsorption models and factors influencing removal, Water Res. 170 (2020), 115362.
[17] E. Çermikli, F. Şen, E. Altıok, J. Wolska, P. Cyganowski, N. Kabay, M. Yüksel, Performances of novel chelating ion exchange resins for boron and arsenic removal from saline geothermal water using adsorption-membrane filtration hybrid process, Desalination 491 (2020), 114504.
[18] P. Dorji, J. Choi, D.I. Kim, S. Phuntsho, S. Hong, H.K. Shon, Membrane capacitive deionisation as an alternative to the 2nd pass for seawater reverse osmosis desalination plant for bromide removal, Desalination 433 (2018) 113–119.
[19] H. Zhang, Y. Ruan, Y. Feng, M. Su, Z. Diao, D. Chen, L. Kong, Solvent-free hydrothermal synthesis of gamma-aluminum oxide nanoparticles with selective adsorption of Congo red, J. Colloid Interface Sci. 536 (2019) 180–188.
[20] Y. Cardona, S.A. Korili, A. Gil, A nonconventional aluminum source in the production of alumina-pillared clays for the removal of organic pollutants by adsorption, Chem. Eng. J. 425 (2021), 130708.
[21] M. Väärtnõu, E. Lust, Adsorption of bromide ions at the Bi| gamma-valerolactone and Bi| propylene carbonate interfaces, J. Electroanal. Chem. 851 (2019), 113438.
[22] A.I. Osman, J.K. Abu-Dahrieh, M. McLaren, F. Laffir, P. Nockemann, D. Rooney, A facile green synthetic route for the preparation of highly active γ-Al2O3 from aluminum foil waste, Sci. Rep. 7 (1) (2017) 1–11.
[23] A. El-Amir, M. Ewais, R. Abdel-Aziem, A. Ahmed, H. El-Anadouli, Nano-alumina powders/ceramics derived from aluminum foil waste at low temperature for various industrial applications, J. Environ. Manag. 183 (2016) 121–125.
[24] G. Murambasvina, C. Mahamadi, Effective fluoride adsorption using water hyacinth beads doped with hydrous oxides of aluminium and iron, Groundw. Sustain. Dev. 10 (2020), 100302.
[25] N. Zhu, J. Qiao, Y. Ye, T. Yan, Synthesis of mesoporous bismuth-impregnated aluminum oxide for arsenic removal: adsorption mechanism study and application to a lab-scale column, J. Environ. Manag. 211 (2018) 73–82.
[26] G. Lee, C. Chen, S.T. Yang, W.S. Ahn, Enhanced adsorptive removal of fluoride using mesoporous alumina, Microporous Mesoporous Mater. 127 (1–2) (2010) 152–156.
[27] B. Ekka, R.S. Dhaka, R.K. Patel, P. Dash, Fluoride removal in waters using ionic liquid-functionalized alumina as a novel adsorbent, J. Clean. Prod. 151 (2017) 303–318.
[28] M. Gómez, J. Pizarro, X. Castillo, C. Díaz, A. Ghisolfi, M. de Lourdes Chávez, J. Arenas-Alatorre, Preparation of mesoporous γ-Al2O3 with high surface area from an AlOOH extract of recycling biomass ash, J. Environ. Chem. Eng. 9 (5) (2021), 105925.
[29] S. Ferdowsi, A. Salem, S. Salem, Spectrophotometrical analysis for fabrication of pH-independent nano-sized γ-alumina by dealumination of kaolin and precipitation in the presence of surfactant composites, Spectrochim. Acta A Mol. Biomol. Spectrosc. 218 (2019) 109–118.
[30] G. Lee, W. Lee, Adsorption of uranium from groundwater using heated aluminum oxide particles, J. Water Process Eng. 40 (2021), 101790.
[31] H. Zhang, Y. Ruan, Y. Feng, M. Su, Z. Diao, D. Chen, L. Kong, Solvent-free hydrothermal synthesis of gamma-aluminum oxide nanoparticles with selective adsorption of Congo red, J. Colloid Interface Sci. 536 (2019) 180–188.
[32] S. Banerjee, S. Dubey, R.K. Gautam, M.C. Chattopadhyaya, Y.C. Sharma, Adsorption characteristics of alumina nanoparticles for the removal of hazardous dye, Orange G from aqueous solutions, Arab. J. Chem. 12 (8) (2019) 5339–5354.
[33] P. Colomban, Structure of oxide gels and glasses by infrared and Raman scattering, J. Mater. Sci. 24 (8) (1989) 3011–3020.

[34] M.A. Zamorategui, R.N. Ramírez, R.J.M. Martínez, M.A.H. Serafín, Synthesis and characterization of gamma alumina and compared with an activated charcoal on the fluoride removal from potable well water, Acta Univ. 26 (2) (2016) 30–35.
[35] T. Basu, K. Gupta, U.C. Ghosh, Performances of as (V) adsorption of calcined (250 C) synthetic iron (III)–aluminum (III) mixed oxide in the presence of some groundwater occurring ions, Chem. Eng. J. 183 (2012) 303–314.
[36] T.A.G.O. Tuguhiro, et al., XPS study from a clean surface of Al2O3 single crystals, Procedia Eng. 216 (2017) 175–181.
[37] T. Rabung, T. Stumpf, H. Geckeis, R. Klenze, J.I. Kim, Sorption of Am (III) and Eu (III) onto γ-alumina: experiment and modelling, Radiochim. Acta 88 (9–11) (2000) 711–716.
[38] M.L. Guzman-Castillo, F. Hernandez-Beltran, J.J. Fripiat, A. Rodriquez-Hernández, R.G. de León, J. Navarrete-Bolanos, X. Bokhimi, Physicochemical properties of aluminas obtained from different aluminum salts, Catal. Today 107 (2005) 874–878.
[39] S. Tabesh, F. Davar, M.R. Loghman-Estarki, The effects of chelating agent type on the morphology and phase evolutions of alumina nanostructures, Ceram. Int. 43 (13) (2017) 10247–10252.
[40] A. Osman, J. Abu-Dahrieh, M. McLaren, F. Laffir, P. Nockemann, D. Rooney, A facile green synthetic route for the preparation of highly active γ-Al2O3 from aluminum foil waste, Sci. Rep. 7 (1) (2017) 1–11.
[41] W. Bouguerra, A. Mnif, B. Hamrouni, M. Dhahbi, Boron removal by adsorption onto activated alumina and by reverse osmosis, Desalination 223 (1–3) (2008) 31–37.
[42] C.-P. Huang, W. Stumm, Specific adsorption of cations on hydrous γ-Al2O3, J. Colloid Interface Sci. 43 (2) (1973) 409–420, https://doi.org/10.1016/0021-9797(73)90387-1.
[43] E. Nariyan, N. Aravindakshan, Q.J. Yu, Q. Li, Removal of iodides and bromides at parts per million concentrations using a novel bismuth composite material, Mater. Today Sustain. 10 (2020), 100054.
[44] C. Gong, Z. Zhang, Q. Qian, D. Liu, Y. Cheng, G. Yuan, Removal of bromide from water by adsorption on silver-loaded porous carbon spheres to prevent bromate formation, Chem. Eng. J. 218 (2013) 333–340.
[45] S.G. Eggermont, R. Prato, X. Dominguez-Benetton, J. Fransaer, Metal removal from aqueous solutions: insights from modeling precipitation titration curves, J. Environ. Chem. Eng. 8 (1) (2020), 103596.
[46] S. Liu, G. Cheng, Y. Xiong, Y. Ding, X. Luo, Adsorption of low concentrations of bromide ions from water by cellulose-based beads modified with TEMPO-mediated oxidation and Fe (III) complexation, J. Hazard. Mater. 384 (2020), 121195.
[47] E. Van Eynde, J.C. Mendez, T. Hiemstra, R.N. Comans, Boron adsorption to ferrihydrite with implications for surface speciation in soils: experiments and modeling, ACS Earth Space Chem. 4 (8) (2020) 1269–1280.
[48] M. Jaouadi, S. Hbaieb, H. Guedidi, L. Reinert, N. Amdouni, L. Duclaux, Preparation and characterization of carbons from β-cyclodextrin dehydration and from olive pomace activation and their application for boron adsorption, J. Saudi Chem. Soc. 21 (7) (2017) 822–829.
[49] S. Kashiwakura, H. Kubo, Y. Kumagai, H. Kubo, K. Matsubae-Yokoyama, K. Nakajima, T. Nagasaka, Removal of boron from coal fly ash by washing with HCl solution, Fuel 88 (7) (2009) 1245–1250.
[50] E. Babiker, M.A. Al-Ghouti, N. Zouari, G. McKay, Removal of boron from water using adsorbents derived from waste tire rubber, J. Environ. Chem. Eng. 7 (2) (2019), 102948.
[51] W. Bouguerra, A. Mnif, B. Hamrouni, M. Dhahbi, Boron removal by adsorption onto activated alumina and by reverse osmosis, Desalination 223 (1–3) (2008) 31–37.
[52] Z. Wang, K. Ma, Y. Zhang, X. Zhang, H.H. Ngo, J. Meng, L. Du, High internal phase emulsion hierarchical porous polymer grafting polyol compounds for boron removal, J. Water Process Eng. 41 (2021), 102025.
[53] H.K. Afolabi, M.M. Nasef, N.A.H.M. Nordin, T.M. Ting, N.Y. Harun, A.A.H. Saeed, Isotherms, kinetics, and thermodynamics of boron adsorption on fibrous polymeric chelator containing glycidol moiety optimized with response surface method, Arab. J. Chem. 14 (12) (2021), 103453.
[54] B. Heibati, K. Yetilmezsoy, M.A. Zazouli, S. Rodriguez-Couto, I. Tyagi, S. Agarwal, V.K. Gupta, Adsorption of ethidium bromide (EtBr) from aqueous solutions by natural pumice and aluminium-coated pumice, J. Mol. Liq. 213 (2016) 41–47.
[55] E.S. Pouya, H. Fatoorehchi, M. Foroughi-Dahr, Batch removal of Pb (II) ions from aqueous medium using gamma- Al2O3nanoparticles/ethyl cellulose adsorbent fabricated via electrospinning method: an equilibrium isotherm and characterization study, Pol. J. Chem. Technol. 20 (2) (2018).
[56] M. Wiśniewska, K. Wrzesińska, M. Wawrzkiewicz, S. Chibowski, T. Urban, O. Goncharuk, V.M. Gun'ko, Alumina-silica-titania adsorbent for hazardous azo and phtalocyanine dyes removal from textile baths and wastewaters–the impact of ionic surfactants, Physicochem. Probl. Miner. Process. 56 (2020).
[57] Y.S. Ho, Review of second-order models for adsorption systems, J. Hazard. Mater. 136 (3) (2006) 681–689.
[58] Y. Li, X. Zhang, P. Zhang, X. Liu, L. Han, Facile fabrication of magnetic bio-derived chars by co-mixing with Fe3O4 nanoparticles for effective Pb2+ adsorption: properties and mechanism, J. Clean. Prod. 262 (2020), 121350.
[59] Z. Wang, Y. Jia, W. Song, X. Li, K. Xu, Z. Wang, Optimization of boron adsorption from desalinated seawater onto UiO-66-NH2/GO composite adsorbent using response surface methodology, J. Clean. Prod. 300 (2021), 126974.
[60] M.K. Shetty, K.V. Karthik, J.H. Patil, S.M. Shekhar, Equilibrium removal, isotherm and kinetic studies of chromium (VI) adsorption onto biopolymers from aqueous solution: a comparative study, Mater. Today: Proc. 49 (2022) 891–897.
[61] X. Zhang, L. Yan, J. Li, H. Yu, Adsorption of heavy metals by l-cysteine intercalated layered double hydroxide: kinetic, isothermal and mechanistic studies, J. Colloid Interface Sci. 562 (2020) 149–158.
[62] P. Priyadarshini, T. Ricciardulli, J.S. Adams, Y.S. Yun, D.W. Flaherty, Effects of bromide adsorption on the direct synthesis of H2O2 on pd nanoparticles: formation rates, selectivities, and apparent barriers at steady-state, J. Catal. 399 (2021) 24–40.
[63] H. Azad, M. Mohsennia, C. Cheng, A. Amini, Facile fabrication of PVB-PVA blend polymer nanocomposite for simultaneous removal of heavy metal ions from aqueous solutions: kinetic, equilibrium, reusability and adsorption mechanism, J. Environ. Chem. Eng. 9 (5) (2021), 106214.
[64] C. Irawan, J.C. Liu, C.C. Wu, Removal of boron using aluminum-based water treatment residuals (Al-WTRs), Desalination 276 (1–3) (2011) 322–327.
[65] M.A. Al-Ghouti, N.R. Salih, Application of eggshell wastes for boron remediation from water, J. Mol. Liq. 256 (2018) 599–610.
[67] D.İ. Çifçi, S. Meriç, A review on pumice for water and wastewater treatment, Desalin. Water Treat. 57 (39) (2016) 18131–18143.